ELSEVIER

Journal of Nuclear Materials 290–293 (2001) 653–657

journal of nuclear materials

www.elsevier.nl/locate/jnucmat

# Energy flux measurements in a steady-state discharge at PSI-2

B. Koch *, W. Bohmeyer, G. Fussmann, P. Kornejew, H.-D. Reiner

*Max-Planck-Institut für Plasmaphysik, EURATOM Association, Bereich Plasmadiagnostik, Mohrenstraße 41, D-10117 Berlin, Germany*

**Abstract**

A newly developed heat flux detector for direct measurement of the energy flux to a floating or biased target is presented. The detector has been used to measure the plasma sheath transmission factor ($\gamma$) for different gases as a function of the electron temperature. The determined values are in the range of $7 < \gamma < 17$; they agree roughly with those theoretical predictions [G.A. Emmert, R.M. Wieland, A.T. Mense, J.N. Davidson, Phys. Fluids 23(4) (1980); H. Kimura, H. Maeda, N. Ueda, M. Seki, H. Kawamura, S. Yamamoto, M. Nagami, K. Odajima, S. Sengoku, Y. Shimomura, Nucl. Fusion 18(9) (1978); R.V. Manos, D.M. Budny, S.A. Cohen, J. Vac. Sci. Technol. A 1 (1983); P.C. Stangeby, J. Phys. D 15 (1982); P.C. Stangeby, Phys. Fluids 27(3) 1984] that include the recombination term. 

*Keywords:* Heat flux; Flux plasma; Boundary sheath

## 1. Introduction

Since the energy flux to the various surfaces in fusion devices is one of the major design issues there is also a need for precise and easy measurement techniques. For the areas of maximum heat load, e.g. divertor plates, probably only thermographic methods will be applicable. On the other hand there are other areas which receive lower heat fluxes and cannot be easily observed by optical methods. Previously used sensors, like bolometers or thermometers, in general were optimised for large peak loads and fast rise times [12,6]. This of course implies that these detectors will be applied for pulsed discharges.

Our newly developed detector described in the following is a water cooled sensor of moderate rise time which may be used also in long pulse (or even stationary) discharges as being planned for ITER or the stellarator W7-X. It is very robust and the obtained measurements can be easily interpreted. First tests and calibration of this detector were performed by means of a pulsed high energy laser. Succeeding plasma measurements were performed at the stationary plasma generator PSI-2. As a first application a quantity of fundamental interest, the sheath transmission factor, was determined as a function of electron temperature in D-, He- and Ar-plasmas and compared with theory.

## 2. The PSI-2 facility

The PSI-2 plasma generator is a stationary high current arc discharge confined by an axial magnetic field. The plasma is produced between a heated $LaB_6$ cathode and a hollow anode made from copper. The plasma generated in this region streams along the magnetic field lines through a differential pumping stage into a target chamber [1] where most of the plasma wall interaction studies and also the heat flux measurements described here are performed. The plasma parameters in this region were determined by means of a movable Langmuir double probe. For most discharge conditions hollow profiles of density and temperature, showing a flat central region, are found. It was this central region that we used for testing the detector and measurements of the sheath transmission factor.

* Corresponding author.

*E-mail address:* bkoch@albert.physik.hu-berlin.de (B. Koch).

0022-3115/01/$ - see front matter 
PII: S0022-3115(00)00597-3

## 3. The heat flux detector

The principle of the detector is based on the measurement of the temperature difference occuring between its central region ($r = 0$) and the outer cooled boundary ($r = R = 5$ mm) when being exposed to an energy flux perpendicular to its surface (see Fig. 1). For this purpose two thermocouples are arranged in opposite directions. One couple is formed by the central copper wire and the Cu–Ni-foil measuring the high temperature in the core region. The second thermocouple measures the temperature of the Cu–Ni-foil at its connection to the cooling head (Cu). When a stationary temperature distribution is attained the temperature difference is directly proportional to the applied heat flux.

Assuming a homogeneous flux density $S$ over the active area of the detector the stationary temperature profile is described by the 1D heat conduction equation which reads in polar-coordinates:

$$\frac{\partial^2 T}{\partial r^2} + \frac{1}{r}\frac{\partial T}{\partial r} + \frac{S}{\lambda d} = 0, \tag{1}$$

where $\lambda$ is the heat conductivity of the sensor material and $d = 0.1$ mm the thickness of the foil. Solving this equations for the boundary conditions:

*Radial symmetry*:

$$\left.\frac{\partial T}{\partial r}\right|_{r=0} = 0. \tag{2}$$

*Thermal conductance* ($\alpha$) *between the foil border and the cooling head at temperature* $T_0$:

$$-\lambda \left.\frac{\partial T}{\partial r}\right|_{r=R} = \alpha(T(R) - T_0). \tag{3}$$

The temperature difference between the two thermocouples is obtained to

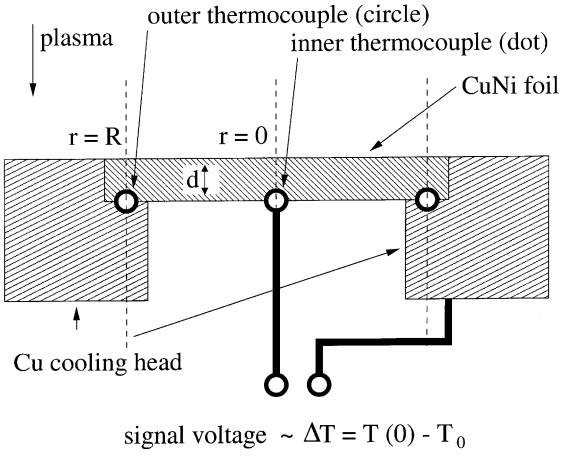


Fig. 1. Principle of the detector.

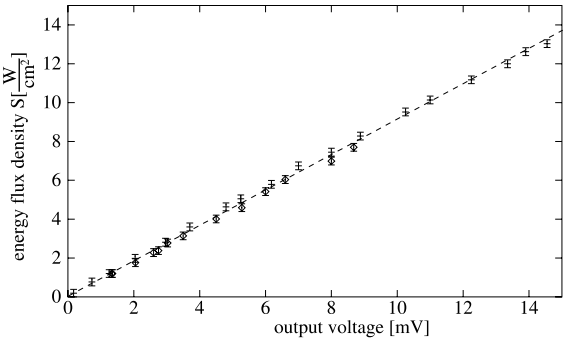


Fig. 2. Linearity of the output relation: energy flux density vs. detector output voltage (data from two successive calibrations).

$$\Delta T := T(0) - T_0 = \left[\left(\frac{1}{2\alpha} + \frac{R}{4\lambda}\right)\frac{R}{d}\right] S. \tag{4}$$

For sufficiently small $\Delta T$ a linear output voltage of the thermocouples can be assumed. This could be confirmed by means of a high energy laser beam applied to the sensor (see Fig. 2).

As a further test we are interested in the temporal behaviour of the signal. Theoretically this is obtained by solving the time-dependent heat conduction equation

$$\frac{\partial T}{\partial t} = \frac{\lambda d}{\rho c d}\left[\frac{\partial^2}{\partial r^2} + \frac{1}{r}\frac{\partial}{\partial r}\right] T \tag{5}$$

with the specific heat $c$, and the mass density $\rho$ of the sensor. A separation ansatz leads to an exponential series

$$T(t, r) = \sum_n^{\infty} C_n(r)\ \exp\left(-\mu_n^2 t\right) \tag{6}$$

with the time constants $\tau_n := \mu_n^{-2}$. The eigenvalues $\mu_n$ are found from the equation

$$\mu_n \frac{J_1\left(\sqrt{\rho c/\lambda}\,\mu_n R\right)}{J_0\left(\sqrt{\rho c/\lambda}\,\mu_n R\right)} = \frac{\alpha}{\sqrt{\rho c \lambda}}, \tag{7}$$

where $J_0, J_1$ are Bessel functions. For $n = 0$ the longest time constant $\tau_0$, characterising the detector response time, is obtained (see Fig. 3).

Varying the detector radius $R$, the thickness $d$ of the sensitive disc or its material allows to adapt the detector to the envisaged measurements. High sensitivity calls for a large radius, thus reducing the spatial resolution and increasing the response time.

## 4. Calibration

An absolute calibration by means of a high repetition rate, long pulse YAG laser system was performed

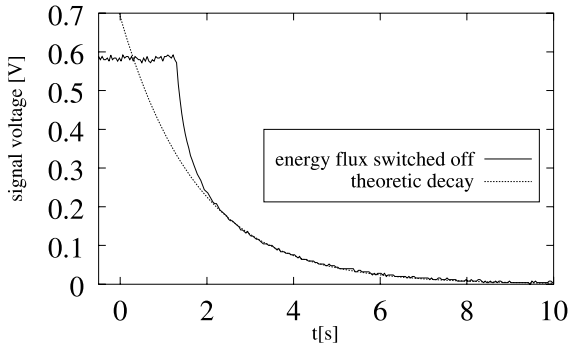


Fig. 3. Detector signal after switching off the laser compared to a single exponential decay with $\tau_0 = 1.8$ s. The deviations can be modeled using Eq. (6).

(Fig. 2). The parallelised output light of the laser (optical fibre) was alternatively directed to the detector or a combination of a diaphragm and a commercial power meter yielding the power flux density of the beam. In order to obtain the power flux density absorbed by the detector the absorption coefficient (65%) of the Cu–Ni-foil at the laser wavelength at 1064 nm was determined with a spectral photometer (Perkin Elmer Lambda 900).

The results of the calibration (Fig. 2) show the expected linear dependence but differ otherwise from calibration data obtained in direct plasma measurements. The time constant of the sensor (see Fig. 3) $\tau_0 = 1.8$ s was also determined with the same setup. As it is to be seen from Fig. 3 the temporal decay of the signal is asymptotically well described by a single exponential – in full agreement with Eq. (6).

## 5. The sheath transmission factor $\gamma$

This important quantity is defined by the relation

$$\gamma := \frac{\text{energy flux density}}{\text{reference energy flux density}} = \frac{S}{T_e j_i / e}. \tag{8}$$

The actual energy influx is compared to a reference energy flux density determined by the electron temperature $T_e$ and the ion saturation current density $j_i$. Well established contributions to the energy flux density are those originating from the acceleration of the ions in the sheath and pre-sheath potentials, the convectively transmitted thermal energies by ions and electrons, and the energy released by recombination at the surface. The resulting theoretical expression for $\gamma$ is given by Eq. (9). Smaller effects due to secondary electron emission [9,7] or those caused by deviations from Maxwellians in the pre-sheath or source regions [8] are not considered here ([2,5,6,10,11]). For small $T_e$ (i.e. $\leqslant 2E_{ion}$) the recombination term (last bracket in (9)) yields a very significant contribution. This statement is fully confirmed by our measurements shown in Figs. 5–7. The corresponding energy transferred to the surface as a result of recombination is given by the ionisation energy $E_{ion}$ minus the work function $W$ of the surface material. If the considered atoms recombine further to molecules (e.g. in hydrogen or deuterium plasmas) half of the corresponding dissociation energy $E_{diss}$ must be added. Moreover, the energy reflection coefficient $R_E$ can be important. In particular for light ions at low energies this coefficient can be significant [13] and reduce the first term in Eq. (9) considerably.

$$\begin{aligned}\gamma_{\text{theo}} = & \underbrace{\left\{\frac{1}{2}\right\}}_{\text{pre-sheath potential drop}} \underbrace{-\frac{1}{2}\ln\left[\left(2\pi\frac{m_e}{m_i}\right)\left(1+\frac{T_i}{T_e}\right)\right]\Big\}(1-R_E)}_{\text{ion acceleration in the floating potential}} \\ & + \underbrace{\left\{2\frac{T_i}{T_e}(1-R_E)+2\right\}}_{\text{ion and electron thermal energy}} + \underbrace{\left\{\frac{E_{ion}-W+\frac{1}{2}E_{diss}}{T_e}\right\}}_{\text{recombination}}\end{aligned} \tag{9}$$

## 6. Experimental results and discussion

Before conducting the experiments in the PSI-2 device the detector and the manipulator were covered with BN ceramics to certify that only the active area is in contact with the plasma. Hence, the detector can also be used as a probe to determine the floating potential and the ion saturation current. This resulted in a total detector diameter of 40 mm compared to an active diameter of 10 mm. In addition, a Langmuir probe was attached to the sensor to determine independently the plasma parameters under the (disturbed) conditions prevailing during the energy flux measurements. Measurements were performed in $D_2$, He and Ar discharges ($1.5 < T_e < 7$ eV) under steady state conditions. The ion saturation current density $j_i$ could be determined by the Langmuir probe and by the detector as well. Energy flux density $S$ and the total detector current were measured as a function of the biasing voltage $U_B$. The function $S(U_B)$ determined this way is shown in Fig. 4. As a generalisation of Eq. (9) for arbitrary $U_B$ and the plasma potential at $U_P$ this energy flux is given by the equation

$$\begin{aligned}S(U_B) = & \underbrace{\left(\frac{1}{2}T_e + e(U_P - U_B)\right)(1-R_E)j_i/e}_{\text{ion acceleration in the pre-sheath potential}} \\ & + \underbrace{\left(E_{ion} - W + \frac{1}{2}E_{diss}\right)j_i/e}_{\text{recombination}} \\ & + \underbrace{\left(2T_i(1-R_E) + 2\sqrt{\frac{m_i}{2\pi m_e}}\exp\left(\frac{e(U_B-U_P)}{2T_e}\right)T_e\right)j_i/e}_{\text{thermal energy}},\end{aligned} \tag{10}$$

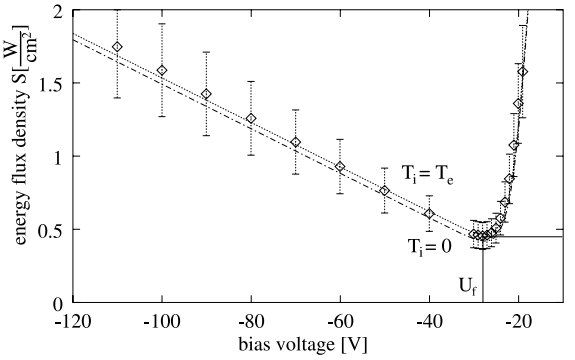


Fig. 4. Measured energy flux density to a biased target in argon in comparison with theoretical curves ($\Gamma_i = 1.2 \times 10^{19}$ m$^{-2}$ s$^{-1}$, $T_e = 1.8$ eV) according to Eq. (10).

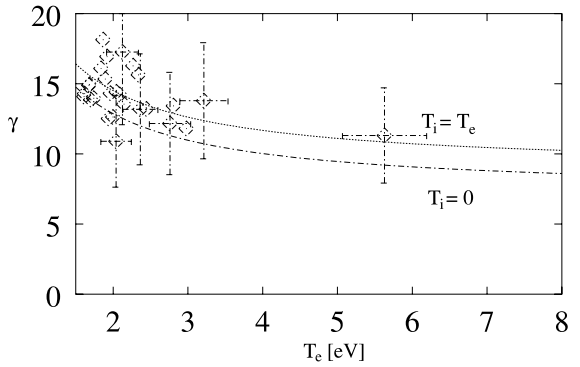


Fig. 5. Sheath transmission factor $\gamma$ in deuterium vs. $T_e$, theoretical curves (Eq. (9)) and experimental data. $T_e$ was inferred from Langmuir Probe data, $j_i$ and $S$ were measured using the energy flux detector.

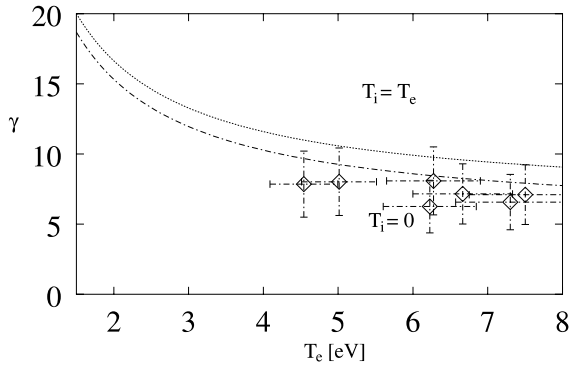


Fig. 6. Sheath transmission factor in helium, similar to Fig. 5.

which (for $R_E = 0$) reaches a minimum when attaining the floating potential $U_f$ in agreement with the experimental results shown in Fig. 4.

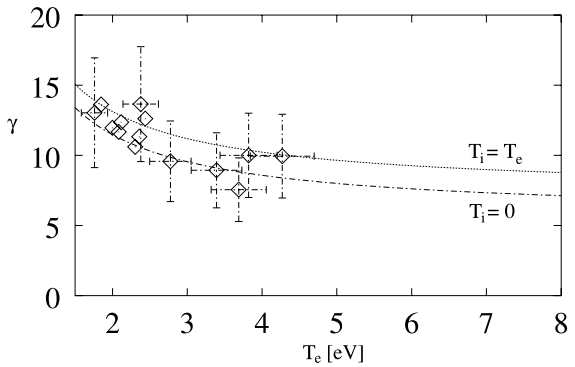


Fig. 7. Sheath transmission factor in argon, similar to Fig. 5.

We used the ion saturation part of the detector characteristics for calibrating energy and particle flux densities with respect to each other. By comparing with the laser calibration data (see Fig. 2) we noticed some inconsistency, possibly caused by the uncertainty in determining the proper active area in the latter case. There is a lack of data for the $R_E$ coefficients for the actual energy range needed in our case. However, there are indications that in case of argon $R_E = 0$ is reasonable approximation [4,14]. On the basis of this assumption we determined the $R_E$ values for deuterium and helium by comparison to the calibrations obtained for argon. For both we observed an $R_E$ of 20%. Excellent agreement between the Langmuir probe and detector saturation currents was found for deuterium and helium. In argon, however, a difference of 20% was noted. The reason of this deviation is most likely due to the large gyro radii of argon ions, being comparable with the size of the detector. The ion temperature according to earlier experiments is approximately $T_i \approx 0.5T_e$ [3]. Fortunately, the influence of $T_i$ on $\gamma$ is rather weak as may be seen from the figures where the two extreme cases $T_i = 0$ and $T_i = T_e$ are plotted for the theoretical cases. The results of our measurements are shown in Figs. 5–7 together with theoretical lines according to Eq. (9). The values of $\gamma$ for helium are systematically lower than predicted by theory. The flat $T_e$ dependence found here suggests an additional energy loss channel during wall contact. This could possibly be ascribed to the metastable triplet state of the He-neutrals.

## 7. Summary

The new heat flux detector is able to deliver reliable data of local energy flux densities. Steady-state heat fluxes as large as $5 \times 10^4$ W m$^{-2}$ could be measured. Furthermore, this new sensor allowed us to perform (to our knowledge for the first time) a systematic study of the sheath transmission factor. Results are in agreement

with theory within the experimental uncertainty of about ~30%. An essential contribution to $\gamma$ is due to the recombination term (see Eq. (9)) often neglected in the older literature.

## References

[1] H. Behrend et al., in: Proceedings of the 21st EPS Conference on Control Fusion and Plasma Physics, 1994, p. 1328–1331.
[2] G.A. Emmert, R.M. Wieland, A.T. Mense, J.N. Davidson, Phys. Fluids 23 (4) (1980).
[3] O. Jensen, Messungen der Ionentemperatur und Stroemungsgeschwindigkeiten in einem Plasma mit linearer Magnetfeldkonfiguration, Diplomarbeit, Humboldt-Universitaet zu, Berlin, 1998.
[4] H. Kersten, E. Stoffels, W.W. Stoffels, M. Otte, C. Sambal, H. Deutsch, R. Hippler, J. Appl. Phys. 87 (8) (2000).
[5] H. Kimura, H. Maeda, N. Ueda, M. Seki, H. Kawamura, S. Yamamoto, M. Nagami, K. Odajima, S. Sengoku, Y. Shimomura, Nucl. Fus. 18 (9) (1978).
[6] R.V. Manos, D.M. Budny, S.A. Cohen, J. Vac. Sci. Technol. A 1 (1983).
[7] L.A. Schwager, Phys. Fluids B 5 (2) (1993).
[8] L.A. Schwager, C.K. Birdsall, Phys. Fluids B 2 (5) (1990).
[9] L.A. Schwager, W.L. Hsu, D.M. Tung, Phys. Fluids B 5 (2) (1993).
[10] P.C. Stangeby, J. Phys. D 15 (1982).
[11] P.C. Stangeby, Phys. Fluids 27 (3) (1984).
[12] P.C. Stangeby, G.M. McCracken, S.K. Erents, J.E. Vince, R. Wilden, J. Vac. Sci. Technol. A 1 (2) (1983).
[13] T. Tabata, R. Ito, Y. Itikawa, N. Itoh, K. Morita, At. Data Nucl. Data Tables 28 (3) (1983).
[14] H. Toyoda, H. Sugai, J. Plasma Fus. Res. 75 (1999).